Optimal Planar Array Architecture for Full-Dimensional Multi-user Multiple-Input Multiple-Output with Elevation Modeling

Alidu Abubakari, Sabogu-Sumah Raymond, and Han-Shin Jo

Research interest in three-dimensional multiple-input multiple-output (3D-MIMO) beamforming has rapidly increased on account of its potential to support high data rates through an array of strategies, including sector or user-specific elevation beamforming and cell-splitting. To evaluate the full performance benefits of 3D and full-dimensional (FD) MIMO beamforming, the 3D character of the real MIMO channel must be modeled with consideration of both the azimuth and elevation domain. Most existing works on the 2D spatial channel model (2D-SCM) assume a wide range for the distribution of elevation angles of departure (eAoDs), which is not practical according to field measurements. In this paper, an optimal FD-MIMO planar array configuration is presented for different practical channel conditions by restricting the eAoDs to a finite range. Using a dynamic network level simulator that employs a complete 3D SCM, we analyze the relationship between the angular spread and sum throughput. In addition, we present an analysis on the optimal antenna configurations for the channels under consideration.

Keywords: Elevation angle of departure, Full-dimensional multiple-input multiple-output (FD-MIMO), Planar Array, Three-dimensional spatial channel model (3D-SCM), Urban macrocell.

Manuscript received Apr. 16, 2016; revised Dec. 19, 2016; accepted Feb. 2, 2017.

Alidu Abubakari (aabubakari32@yahoo.com), Sabogu-Sumah Raymond (rsabogusuma@yahoo.com), and Han-Shin Jo (corresponding author, hsjo@hanbat.ac.kr) are with the Department of Electronic Engineering, Hanbat National University, Daejeon, Rep. of Korea.

I. Introduction

User requirements are rapidly increasing. The limitations of current mobile communication systems have thus compelled researchers to design more advanced and efficient technologies. It is known that the minimum between the total transmit and receive antennas determines the capacity of a single-user multiple-input multiple-output (MIMO) system. On the other hand, in the case of a multi-user MIMO system, the total number of base station (BS) antennas determines the capacity. Thus, the most feasible and simple means of improving system capacity is to increase the BS antennas. The study in [1] proved that vertically deploying antennas enables use of the elevation dimension to achieve up to a 30% system gain. By properly configuring a two-dimensional (2D) antenna array at the BS, network throughput can be improved with three-dimensional (3D) multi-user MIMO techniques without modifying the terminal antenna form factor. Based on this analysis and the results in [1], FD-MIMO employs 2D active antenna array configurations to improve capacity for next-generation wireless networks and services.

A surge has recently occurred in modeling wireless channels that capture both the azimuth and elevation angular resolutions of signal propagation. These are known as 3D channels. Consequently, the wireless research community has been intensively designing and standardizing 3D channel models that can leverage the benefits of both azimuth and elevation beamforming [2]. To evaluate the performance of FD-MIMO, the problem of modeling the elevation spread in the 3D channel is critical. To date, the elevation angle of 3D antenna arrays has been considered for different scenarios by the 3rd Generation Partnership Project (3GPP). However, no complete channel model has been developed for realistic systems; additional measurements must therefore be performed. Several researchers have studied the stochastic characteristics of the

elevation angular range using practical environmental measurements.

Taga's study [3] was based on the channel measurement of the Tokyo urban area at 900 MHz. He postulated that the elevation spread followed a wide dispersive Gaussian distribution. In addition, he observed that both the horizontal and vertical incoming signal angles have a Gaussian distribution with different means and variances. Shafi and others [4], considered the extension of the current spatial channel model (SCM) to factor the 3D space of the MS. Meanwhile, the WINNER+ project [5] recently summarized most available literature on the mobile station (MS)/BS angular spread for both elevation and azimuth, while extending the 2D model to the 3D space. In our previous work [6], we presented results on the performance of FD-MIMO for varying antenna configurations under the urban macro-channel environment. The present work is an extension of that study; here, we consider more practical urban macrocell-channel conditions by restricting the angle of departure (AoD) of all signals.

In this paper, the azimuth channel statistics employed in the spatial channel model [7] are extended to the elevation dimension for implementing a complete 3D channel model. In addition, based on the practical 3D fading channel measurements presented in [8]–[10], we implement an elevation range restriction technique that introduces boundaries to all signals in the elevation domain. Our work then explores the best type of antenna arrangement that can employ the benefits of FD-MIMO via elevation spread modeling. The assumption that the elevation spread is restricted perfectly models the effect of both non-line-of-sight (NLOS) and LOS dominance in urban environment. The results in this paper show that the elevation spread restriction minimizes the interference associated with the angular spread increase, and the vertical antenna configuration (1 × 16) provides the best performance in terms of average cell throughput. Additionally, the horizontal arrangement of elements with a 16 × 1 configuration provides very good performance for cell edge users.

The remainder of this paper is organized as follows. Section II discusses the 3D channel model, which captures the wireless channel propagation effects in both the elevation domain and azimuth domain. Moreover, the channel parameter generation is described. The 3D beamforming technique is explained in Section III, and numerical results are detailed in Section IV. Finally, conclusions are presented in Section V through a summary of results and relevant analysis.

II. System Model

We consider a downlink multi-user network model consisting of Q BS with a total of three sectors per BS ($3Q$ sectors) arranged in a hexagonal grid. It is assumed that all sectors share the same spectrum for the downlink transmission, and each sector contains U uniformly distributed users equipped with N_r linear antennas. The BS is equipped with $N_T(N_V \times N_H)$ planar array elements, while users are equipped with N_R linear antennas. We assume users are associated with the nearest BS with the highest received power (based on pathloss and shadowing).

1. Multi-cell Transmission Model

We focus on a typical macrocell, where the BS height is greater than the large-scale clutter. Furthermore, all users are at the ground level. Non-homogeneity of the building is in terms of both building height and building density. In such a propagation environment, the azimuth dimension has a wider coverage [−60°, 60°] than the elevation because all users are assumed to be located at the ground level. Both elevation dimensions and azimuth dimensions experience rich scattering as proposed by the spatial channel model.

Following the above-described propagation model, the channel between the uth user and the qth BS with transmit power P can be expressed as $\beta_{q,u}\left(P,\varphi_q,\theta_q\right)\mathbf{H}_{q,u}$, where the path gain is given by

$$\beta_{q,u}\left(P,\varphi_q,\theta_q\right)=\sqrt{L_{q,u}G_{q,u}\left(\varphi_q,\theta_q\right)}. \quad (1)$$

Here, $L_{q,u}$ captures the modified COST231 Hata urban pathloss propagation model between the u-th user and the qth BS, while $G_{q,u}(\varphi_q,\theta_q)$ indicates the observed antenna gain at the uth user from the qth BS. The antenna gain $G_{q,u}(\varphi_q,\theta_q)$ is a function of φ_q, which denotes the azimuth angle of the direct line connecting the BS to the u-th user with respect to antenna boresight. Moreover, θ_q is the elevation angle of the direct line, and $\mathbf{H}_{q,u}\in\mathbb{C}^{N_R\times N_T}$ denotes the small-scale fading channel between the user and target BS. Small-scale fading is a function of the angular spread of multipaths in both the elevation domain and azimuth domain. This is modeled using the 3D spatial channel model, which accounts for scatterers in both domains.

A BS with N_T transmit antennas serves U mobile users in a frequency-flat block fading channel. Here, $\mathbf{x}_q$ is an $N_T\times 1$ transmitted signal vector, and $\mathbf{r}_u$ is an $N_R\times 1$ received signal vector of the uth receiver related by

$$\mathbf{r}_u=\sqrt{\frac{P}{N_T}}\beta_{q,u}\mathbf{H}_{q,u}\mathbf{x}_q+\sqrt{\frac{P}{N_T}}\sum_{q'\neq q}\beta_{q',u}\mathbf{H}_{q',u}\mathbf{x}_{q'}+\mathbf{z}_u, \quad (2)$$

where $\mathbf{z}_u\in\mathbb{C}^{N_R\times 1}$ is the additive white Gaussian noise (AWGN) vector with a zero mean and unit covariance $\mathbb{E}[\mathbf{z}\mathbf{z}^{\mathrm{H}}]=Z_o\mathbf{I}_{N_r}$. Here, $(\cdot)^{\mathrm{H}}$ denotes the conjugate transpose

and $\mathbf{I}_{N_r}$ denotes the $N_T \times N_T$ identity matrix. The total transmit power is uniformly distributed over N_T independent substreams, and the transmission rates of each substream are subject to feedback information on the channel quality from a receiver.

The BS employing multiuser MIMO transmission constructs N_T orthonormal beams to the receivers $\{u_k^*\}_{k=1,\ldots,N_T}$, each of which has the highest priority via the beamforming vector $\{\mathbf{f}_k \epsilon \mathbb{C}^{N_T \times 1}\}_{k=1,\ldots,N_T}$. The transmit signal is then

$$\mathbf{x}_q = \mathbf{F}\mathbf{s} = \sum_{k=1}^{N_T} \mathbf{f}_k s_k, \tag{3}$$

where $\mathbf{F} = [\mathbf{f}_1\ \mathbf{f}_2 \cdots \mathbf{f}_{N_T}]$ and $\mathbf{s} = [s_1\ s_2 \cdots s_{N_T}]^{\mathrm{T}}$. The transmitted signal vector s is recovered through a minimum mean square error (MMSE) receiver. The signal-to-interference plus noise ratio (SINR) on the kth stream weighted by $\mathbf{f}_k$ for the uth user is given by

$$\gamma_{u,k} = \mathbf{f}_k^{\mathrm{H}} \mathbf{H}_{q,u}^{\mathrm{H}} \left(\begin{array}{c} \mathrm{Z}_o \mathbf{I}_{N_r} + \\ \sum_{k'=1,k' \neq k}^{N_T} \mathbf{H}_{q,u} \mathbf{f}_{k'} \mathbf{f}_{k'}^{\mathrm{H}} \mathbf{H}_{q,u}^{\mathrm{H}} + \\ \sum_{q'=1,q' \neq q}^{3Q} \mathbf{H}_{q',u} \mathbf{F}\mathbf{F}^{\mathrm{H}} \mathbf{H}_{q',u}^{\mathrm{H}} \end{array} \right)^{-1} \mathbf{H}_{q,u} \mathbf{f}_k. \tag{4}$$

2. Beam and User Selection

Based on the assumption that F is known a priori to receivers, and each receiver has perfect receive channel state information (CSI) $\mathbf{H}_{q,u}$, each receiver evaluates its SINR $\gamma_{u,k}$ and feeds them back to the transmitter. The transmitter assigns s_n to receiver u_k^* with the highest PF priority via the transmit weight vector, $\mathbf{f}_k$. Thus, in the tth time slot, the BS selects a user employing the traditional proportional fair algorithm given by

$$u_k^* = \arg \max_{u=\{1,\ldots,U\}} \frac{\log_2\left(1+\gamma_{u,k}(t)\right)}{\mu_u(t)}, \tag{5}$$

where $\mu_u(t)$ is the average rate of the uth user, and it is updated as

$$\mu_u(t+1) = \begin{cases} \left(1-\dfrac{1}{t_c}\right)\mu_u(t) + \dfrac{1}{t_c} R_u(t) & u = u_k^*, \\ \left(1-\dfrac{1}{t_c}\right)\mu_u(t) & \text{otherwise}, \end{cases} \tag{6}$$

where $R_u(t)$ is the data rate for the uth user scheduled in the tth time slot. The sum rate is given by

$$R = \sum_{k=1}^{N_T} \log_2\left(1+\gamma_{u_k^*,k}(t)\right). \tag{7}$$

3. 2D Active Antenna Array Model

To elucidate the application of the 3D beamforming technique in FD-MIMO, we introduce the antenna configuration employed in this work. The architecture of the transmitter in FD-MIMO is very important because it determines the potential system gain. Our simulator assumes $G_{\max}$ = 14 dB as the maximum directional antenna gain. To determine the azimuth and elevation antenna pattern, we apply (8) and (9), respectively.

$$A_V(\theta) = -\min\left[12\left(\frac{\theta-\theta_{\mathrm{tilt}}}{\theta_{3\mathrm{dB}}}\right)^2, A_m\right], \tag{8}$$

$$A_H(\varphi) = -\min\left[12\left(\frac{\varphi}{\varphi_{3\mathrm{dB}}}\right)^2, A_m\right], \tag{9}$$

where $\theta_{3\mathrm{dB}}$ is defined as the angle between the direction of interest and the boresight of the antenna in the vertical dimension, and $\varphi_{3\mathrm{dB}}$ represents the same in the horizontal domain. $\theta_{3\mathrm{dB}}$ and $\varphi_{3\mathrm{dB}}$ are the 3-dB beamwidths of the vertical and horizontal beams, respectively. A_m = 20 dB is the maximum attenuation, and θ_{tilt} is the electrical tilt angle.

The 3D antenna gain $G(\theta,\varphi)$ is combined as a sum of the horizontal and vertical antenna pattern gains. It is given in (10) as

$$G_{\max} - \min\left\{-\left[A_{E,V}(\theta) + A_{E,H}(\varphi)\right], A_m\right\}. \tag{10}$$

4. Kronecker-Based Discrete Fourier Transform (DFT) Beamspace Preprocessing

In the FD-MIMO beamforming, a directive beam forms such that the beam's angle can be steered by adjusting the relative phase of the signal to each element [11]. Thus, via planar array transmit beamforming, signals can be adjusted to form beam patterns in desired directions to specific users [11]–[13].

The DFT-based beamforming weight-vector codebook, whose beamforming weight-vector code words are actually permuted columns of a DFT matrix, is implemented in [14] [15]. It is considered a standard owing to its simplicity [16]. An interesting DFT codeword feature benefiting the 2D multi-user MIMO is that, as the number of antennas at the BS increases, the corresponding half-power beam width (HPBW) of the DFT beams becomes more narrow [17].

To design a feasible codebook for the 2D uniform planar array (UPA) system, a Kronecker product was introduced [18], [19]. In this design, the final codeword consists of the Kronecker product of two oversampled DFT codewords from both the horizontal and vertical codebooks. Omitting the user and BS notations for simplicity, $\{\mathbf{f}_k\}_{k=0,\ldots,N_T-1}$ is given by

ETRI Journal, Volume 39, Number 2, April 2017
https://doi.org/10.4218/etrij.17.0116.0036

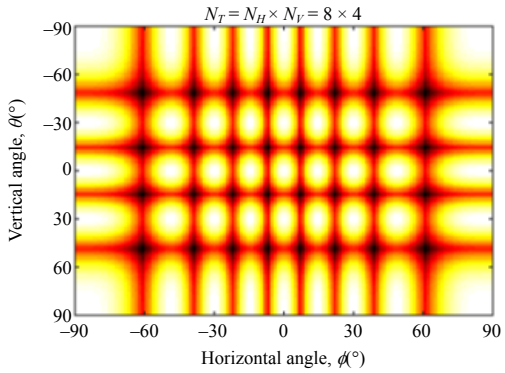

Fig. 1. Beam pattern generated by the DFT matrix for a 32 element antenna.

$$\mathbf{f}_{V,a} = \frac{1}{\sqrt{N_v}}\left[1, e^{\frac{j2\pi a}{N_V}}, \ldots, e^{\frac{j2\pi(N_V-1)a}{N_V}}\right]^{\mathrm{T}}, \tag{11}$$

$$\mathbf{f}_{H,b} = \frac{1}{\sqrt{N_h}}\left[1, e^{\frac{j2\pi b}{N_H}}, \ldots, e^{\frac{j2\pi(N_H-1)b}{N_H}}\right]^{\mathrm{T}}, \tag{12}$$

$$\mathbf{f}_{aN_H+b} = \mathbf{f}_{V,a} \otimes \mathbf{f}_{H,b}, \tag{13}$$

where $a = 0, 1, 2, \ldots, N_V-1$, and $b = 0, 1, 2, \ldots, N_H-1$. Meanwhile, N_V and N_H are the number of codewords in the horizontal and vertical codebooks, respectively, and $\otimes$ represents the Kronecker product. Figure 1 shows the beam pattern for 32 elements (8 × 4) generated with the DFT matrix.

III. Extension from 2D SCM to 3D SCM

To date, the evaluation and standardization of MIMO techniques by 3GPP have been primarily based on 2D channel models from SCM, ITU, and WINNER 2 [20]. The extension from 2D to 3D channel models is published as part of WINNERII/WINNER+ [21], [22]. For generating the elevation angular spread, our 3D model reuses similar azimuth modeling techniques as reported in [21] and [22].

1. Generation of System Narrowband Channel Parameters

To maintain simple spatial channel modeling, the characteristics employed in 2D MIMO are extended to the 3D MIMO. Thus, six paths, each with 20 subpaths, are used to model the multipath effect in both the azimuth and elevation. Let μ_{eAS}, μ_{aAS}, $\sigma_{\mathrm{eAS},q}$, $\sigma_{\mathrm{aAS},q}$ describe the mean elevation angle spread, mean azimuth angle spread, BS elevation spread, and BS azimuth spread, respectively. A Gaussian distribution with variance $\sigma_{\mathrm{eAoD}} = r_{\mathrm{AS}}\sigma_{\mathrm{eAS},q}$ and $\sigma_{\mathrm{aAoD}} = r_{\mathrm{AS}}\sigma_{\mathrm{aAS},q}$ is chosen for the elevation angle of departure (AoD) (σ_{eAoD}) and azimuth AoD (σ_{aAoD}). The proportionality value r_{AS} is close to the measured values in [23]. Higher values of r_{AS} correspond to a greater amount of power being concentrated in small AoD and vice versa.

The AoD values for elevation and azimuth are initially given as $\delta_n \sim N(0, \sigma^2_{\mathrm{eAoD}})$ and $\delta_n \sim N\left(0, \sigma^2_{\mathrm{aAoD}}\right)$, respectively, where n = 1, … , 6. It is evident from practical channel measurements [8] that, for the elevation domain, the LOS direction is not the mean value on account of varying distances between MS's and the BS.

Based on the log-normal relationship established in [24]–[27], the BS elevation spread $\sigma_{\mathrm{aAS},q}$ and BS azimuth spread $\sigma_{\mathrm{eAS},q}$ can be expressed as

$$10\log_{10}(\sigma_{\mathrm{eAS},q}) = \mu_{\mathrm{eAS}} + \varepsilon_{\mathrm{eAS}} C_{1n}, \tag{14}$$

$$10\log_{10}(\sigma_{\mathrm{aAS},q}) = \mu_{\mathrm{aAS}} + \varepsilon_{\mathrm{aAS}} C_{2n}. \tag{15}$$

In (14) and (15), C_{1n} and C_{2n} are zero-mean and unit-variance Gaussian random variables. Similarly, the ε-coefficients are constants representing the lognormal variance of each parameter. For example,

$$\varepsilon_{\mathrm{eAS}} = \mathrm{E}\left[\left(10\log_{10}(\sigma_{\mathrm{eAS},q}) - \mu_{\mathrm{eAS}}\right)^2\right]. \tag{16}$$

The values of μ and ε for the channel under consideration are adapted from [21]. In our work, we introduce a parameter known as the range restriction factor, which is based on results from popular channel measurements. Accordingly, these model the restriction of the elevation AoDs (eAoDs) used in our work. Thus, all BS eAoDs are limited to the ranges in Table 1 for each channel environment.

In the table, 0° denotes the antenna boresight direction, which

Table 1. Environment elevation range spread.

Channel	Elevation range spread $\theta_r = \{(-\alpha°)-(+\alpha°)\}$
Urban NLOS channel	− 10°–10°
Suburban channel	− 10°–80°
Urban LOS channel	0°

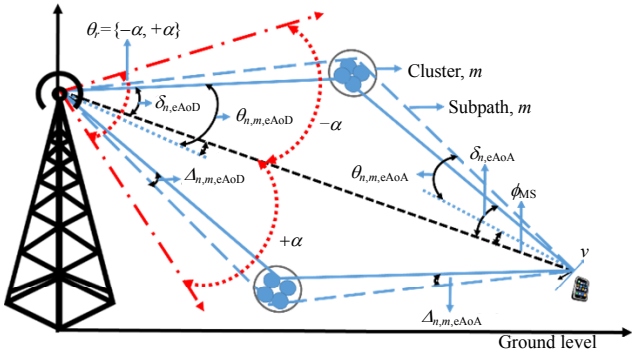

Fig. 2. Elevation BS and MS antenna parameters for the 3D SCM.

serves as the reference direction. The paths departing above the reference have negative eAoDs; those departing below the reference have positive eAoDs, as illustrated in Fig. 2.

2. Generation of Fast-Fading Coefficients

Figure 3 shows the BS and MS antenna parameters for the elevation dimension of the 3D SCM channel. Since similar azimuth parameters are employed for the azimuth, the absolute eAoD and aAoD for the mth ($m = 1, \ldots, M$) subpath of the nth path at the BS with respect to the broadside is given as

$$\theta_{n,m,\mathrm{eAoD}} = \theta + \delta_{n,\mathrm{eAoD}} + \Delta_{n,m,\mathrm{eAoD}}, \tag{17}$$

$$\varphi_{n,m,\mathrm{aAoD}} = \varphi + \delta_{n,\mathrm{aAoD}} + \Delta_{n,m,\mathrm{aAoD}}. \tag{18}$$

It can be observed from practical channel measurements [8] that, for the elevation domain, the LOS direction is not the mean value on account of the varying distances between the MS's and the BS. The generations of $\Delta_{n,m,\mathrm{aAoD}}$ and $\Delta_{n,m,\mathrm{eAoD}}$ are based on the fixed values given in [7], which produce a biased standard deviation equal to two degrees for the typical macrocell case. The channel of the nth path between the uth MS antenna and sth BS antenna is given by

$$h_{u,s,k} = \sqrt{\frac{p_n \sigma_{\mathrm{SF}}}{M}} \sum_{m=1}^{M} \begin{bmatrix} \sqrt{G_{\mathrm{BS}}\left(\theta_{n,m,\mathrm{AoD}}, \varphi_{n,m,\mathrm{AoD}}\right)} \times \\ \exp\left(j\left[kd_s \overline{r_s \phi_{n,m}} + \phi_{n,m}\right]\right) \times \\ \sqrt{G_{\mathrm{MS}}\left(\theta_{n,m,\mathrm{AoA}}, \varphi_{n,m,\mathrm{AoA}}\right)} \times \\ \exp\left(j\left[kd_u \sin\left(\theta_{n,m,\mathrm{AoA}}\right)\right]\right) \times \\ \exp\left(j\begin{bmatrix} k\,||v||\cos\varphi_{n,m,\mathrm{AoA}} \times \\ \cos\left(\theta_{n,m,\mathrm{AoA}} - \theta_v\right)t \end{bmatrix}\right) \end{bmatrix}, \tag{19}$$

where $\overline{r_s \phi_{n,m}} = x_s \cos(\varphi_{n,m,\mathrm{AoD}}) \cos\left(\theta_{n,m,\mathrm{AoD}}\right) + y_s (\cos\varphi_{n,m,\mathrm{AoD}})$ $(\sin\theta_{n,m,\mathrm{AoD}}) + z_s \sin(\varphi_{n,m,\mathrm{AoD}})$. The notations used in (19) are defined in [28], and corresponding values are taken from data in [7].

IV. Numerical Results

In this section, we present our simulation results on the different types of antenna configurations with different elevation modeling techniques to exploit the FD-MIMO performance gain. Table 2 shows the details of the parameters employed in the simulation. The various channel conditions are based on the SCM macrocell scenario as described above and depicted in Fig. 1.

1. SINR and Rate Distribution Results

A preliminary network-level simulation was conducted to evaluate the optimal antenna tilt angle that supports a high SINR, and the average cell throughput in comparison with increasing users. Figure 3(a) shows that, with an increasing number of antennas, the MMSE estimate of the instantaneous SINR worsens. This is due to the equal power per element allocation).

From the system performance shown in Fig. 3(b), a 10°

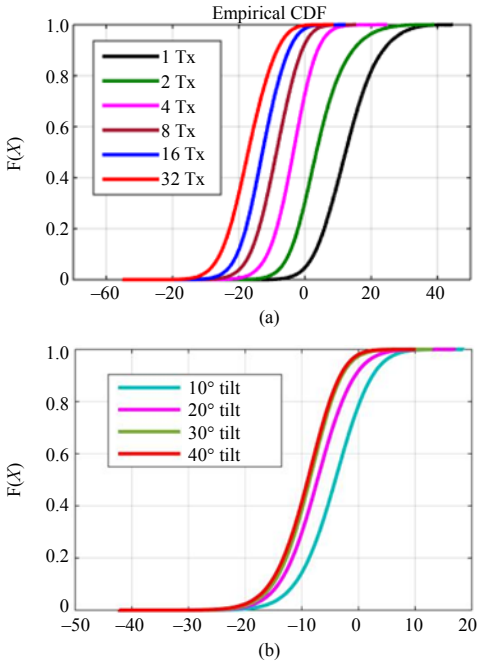

Fig. 3. (a) Instantaneous SINR plot for increasing transmit antenna and (b) CDF of SINR for different antenna tilt values.

Table 2. Simulation parameters.

Parameter	Value
Multi-cell layout	19 cells each with 3 sectors in hexagon layout
Inter-BS site minimum distance	600 m (macro case)
Tx Power	43 dBm
Carrier frequency	2 GHz
Channel model	3D SCM
UE distribution	Uniform
UE speed	3 km/h
Scheduling delay	0 ms
Channel estimation	Ideal without error
UE antenna number	2
BS antenna number	16
Max antenna gain	14 dB
3 dB beamwidth	70°(AZ), 23°(EL)
Antenna element spacing	0.5λ

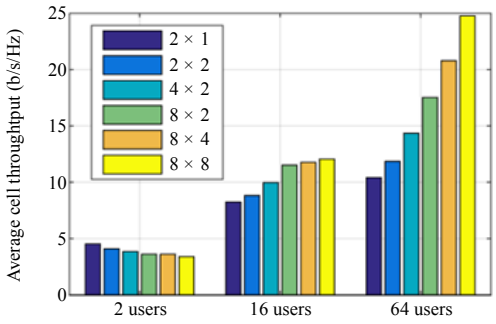

Fig. 4. Throughput analysis in comparison with increasing user cases.

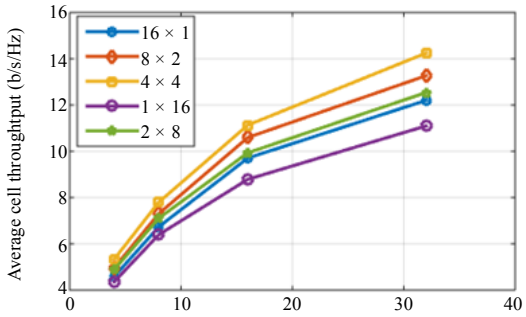

Fig. 5. Effect of increasing the number of users with different antenna configurations.

antenna tilt provides better SINR performance compared to other antenna tilt values. This implies that using a 10° antenna tilt would provide a high SINR (high received signal) for most users. Thus, we employed a 10° antenna tilt for our simulation.

Figure 4 shows that FD-MIMO can obtain all the benefits of the conventional MIMO at a greater scale with the number of users being greater than the number of BS antennas.

2. Result for No Elevation Restriction

The no elevation restriction models a typical urban environment with local scatterers located in the MS vicinity. Typically, the antenna orientation for the transmitter and receiver is defined with respect to the LOS path between the two terminals. The range of directional values for the antenna array is $0° \le \theta \le 90°$. The elevation angular spread ranges from $-180° \le \theta \le 180°$ owing to the fact that no restriction is employed for this scenario.

As shown in Fig. 5, 4 × 4 outperforms all other configurations. This is because of the formation of beams in both elevation and azimuth domains and the user separability (providing high beamforming gain) in both domains. Owing to the antenna tilting and small beamwidth employed in the elevation domain, 4 × 4 provides appropriate beam structures to maintain reduced sector-to-sector and intra-cell interference.

Nevertheless, owing to the large range of eAoDs (due to the lack of elevation restriction), a 1 × 16 antenna configuration would experience high inter-beam interference, thereby limiting the throughput performance. A higher angular spread implies a weak signal case, that is, the lack of a single dominant signal. Owing to the correlation between wideband parameters, this implies a higher delay spread and shadow fading. As shown in Fig. 6, a wider angular spread leads to a lower correlation and high interference, resulting in a low signal received power and thus reduced throughput. This is observed with 16 × 1 and 1 × 16 for both azimuth and elevation configurations of 8°, 15° and 15°, 8°. It is also evident that, for all azimuth/elevation spread configurations, 4 × 4 performs optimally.

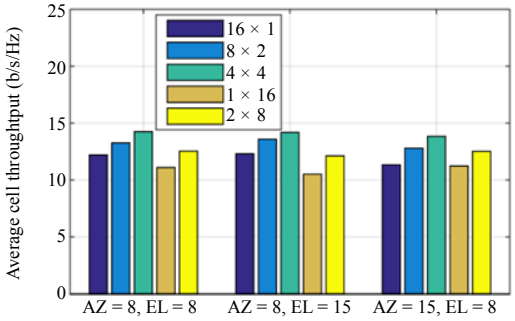

Fig. 6. Angular spread effect for different antenna configurations.

3. Result for Urban with eAoD Restriction

In a typical urban macrocell, the angular spread ranges from $0° \le \theta \le 360°$. However, from the channel measurements, we note that $\theta > 90°$ is rarely observed. Therefore, for the elevation eAoD spread, we used the formulation in Table 1 to restrict the elevation eAoD range to [−10°, 10°] with respect to the LOS path between the two terminals. This implies that the AoDs of all subpaths in the elevation dimension have a small range. This clearly models the NLOS dominance over the rooftop propagation.

As shown in Fig. 7, vertical beamforming dominates the performance trend (1 × 16 > 2 × 8 > 4 × 4 > 8 × 2 > 16 × 1). The elevation domain experiences very narrow pencil beams with high directivity and increased gain on account of the angular restriction. This would eliminate or minimize the possibility of inter-beam interference as a result of beam overlapping and inter-sector interference with adjacent sectors. Nonetheless, owing to the large range of eAoDs (due to the lack of elevation restriction), the 1 × 16 antenna configuration would experience high inter-beam interference, thereby limiting the throughput performance.

4. Result for Suburban Restriction

It was apparent from channel measurements that eAoD's $\theta >$ 90° are rarely observed. Therefore, we implemented an eAoD

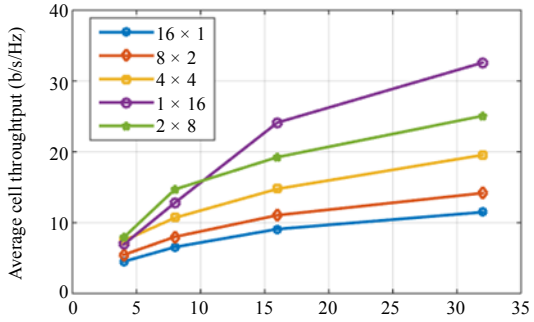

Fig. 7. Effect of increasing the number of users with different antenna configurations.

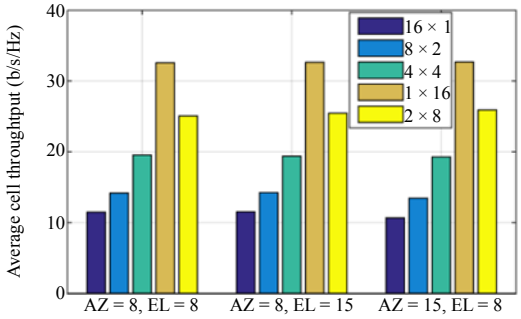

Fig. 8. Angular spread effect for different antenna configurations.

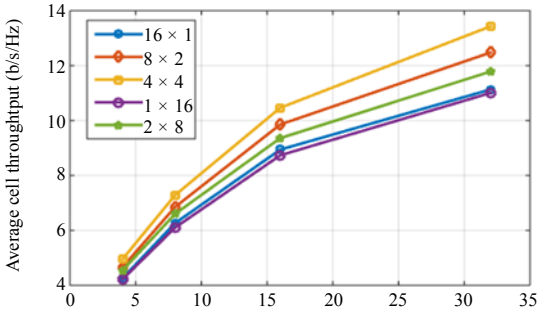

Fig. 9. Effect of increasing the number of users with different antenna configurations.

restriction with the range of [−10°, 80°] with respect to the LOS path between the two terminals. Thus, the eAoDs of all subpaths in the elevation dimension have a wide range.

From Fig. 9, it can be observed that the suburban case with wide eAoD's has the same performance as the case with no elevation restriction.

The 4 × 4 antenna configuration outperformed the other configurations, including vertical (16 × 1) and horizontal (1 × 16) beamforming. This can be attributed to reduced sector-to-sector interference with high user selectivity in the spatial domain.

As observed in Fig. 10 for the different spread scenarios of suburban restriction, a wider angular spacing of 90° in the elevation domain eliminates the interference effect, which

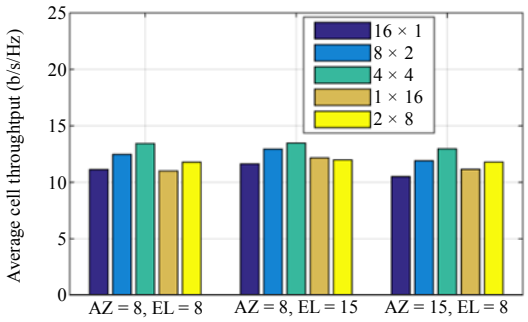

Fig. 10. Angular spread effect for different antenna configurations.

reduces the data throughput observed for the case of no restriction in Fig. 6. Thus, it can be observed that the eAoD restriction eliminates the interference effect caused by the increased angular spread. This effect is also observed in Fig. 8.

5. Result for Urban Restriction with High Elevation LOS

In practical LOS channel measurements, smaller angular spread values were recorded at the BS using directional planar arrays. This can be attributed to the increase in received power due to the main portion of the transmit power arriving from a single direction. In modeling the LOS case, the channel coefficients could therefore be obtained by a single LOS ray direction and scaling down the NLOS components. To implement an elevation angular spread restriction in the urban model, the eAoD range was restricted to [−10°, 10°] with respect to the LOS path between the two terminals. Thus, the AoDs of all subpaths in the elevation dimension had a small range. In this case, all AoDs outside the restricted angular zone were set to the LOS, which, in this case, was 0°. Thus, most AoDs would have been in the LOS direction. This modeled a typical Rician scenario since there existed a dominating AoD component.

Urban restriction with LOS resulted in a dominating elevation beamforming, as can be observed in the Fig. 11 results. This finding is similar to that of the urban case, as shown in Fig. 7. The presence of a dominating signal path in this case, the LOS direction in the elevation dimension results in high throughput via high beam directivity and increased gain. This minimized the inter-beam interference from the beam overlap and consequently minimized interference with adjacent sectors.

Figure 12 shows a similar trend with a 1 × 16 transmit antenna configuration providing better performance, with 8° and 15° being the optimal angular conditions.

6. Cell Edge Performance Analysis

The vertical pattern was fixed and had a narrow HPBW,

ETRI Journal, Volume 39, Number 2, April 2017
https://doi.org/10.4218/etrij.17.0116.0036

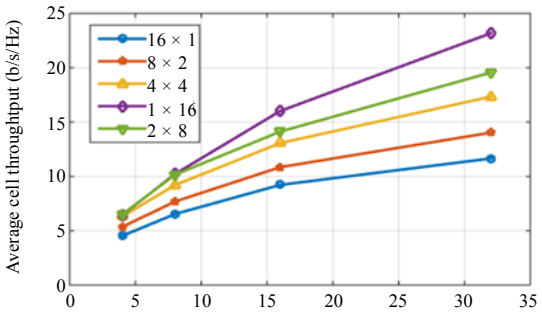

Fig. 11. Effect of increasing the number of users with different antenna configurations.

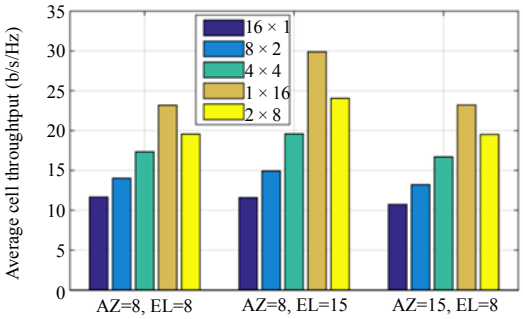

Fig. 12. Angular spread effect for different antenna configurations.

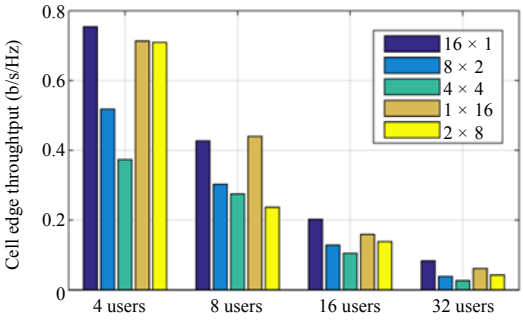

Fig. 13. Cell edge throughput for increasing users.

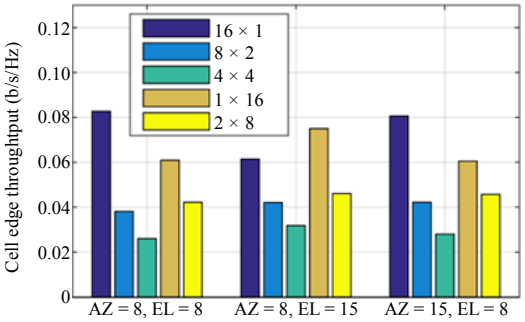

Fig. 14. Cell edge throughput for different angular spread scenarios.

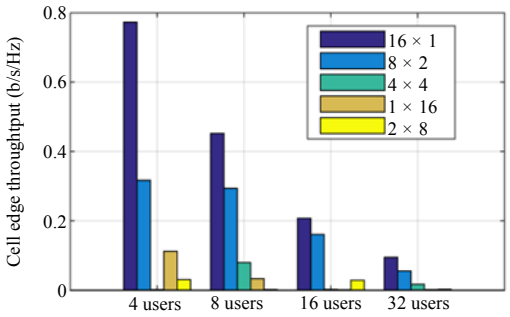

Fig. 15. Cell edge throughput for increasing users.

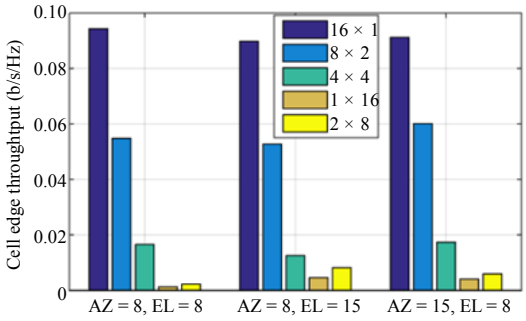

Fig. 16. Cell edge throughput for different angular spread scenarios.

which had to be adequately wide to cover the cell range and sufficiently small to guarantee a high antenna gain. However, in the case of cell edge users, as observed from the above results, a narrow HPBW was not beneficial owing to the fact that most beams were allocated to MS's close to the cell center. As shown in Fig. 13 and Figs. 15 to 20, a broad HPBW employed for the horizontal beamforming (16 × 1) tended to provide better performance for cell edge users, although it also tended to encounter high interference owing to the wide beam formation.

In Fig. 14, for the case of the elevation spread of 15, it is observed that vertical beamforming with a configuration of 1 × 16 provides a higher cell edge throughput. This is because with no elevation spread, the beams spread out omnidirectionally, thus increasing the probability of signals propagating to users.

7. Effect of eAoD Increase on Throughput

For the urban restriction case, the elevation angular spread tended to be small, reflecting the clear dominance over the rooftop propagation mechanism. This can be observed from the performance of [0°, 10°] in the results of Fig. 21.

The reduction in throughput with increasing eAoD spread can be attributed to the increase in interference due to inter-beam interference. There was an increased possibility of sector-to-sector interference, especially in the case of elevation vectorization. Moreover, for the case where all users were located at ground level, the transmission with positive signal directions

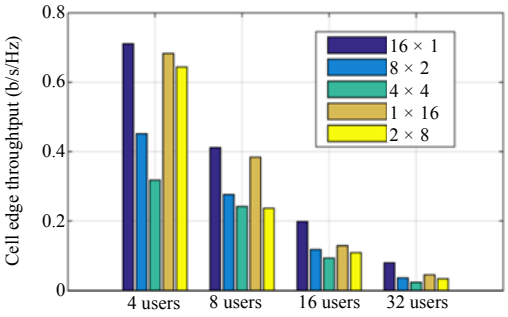

Fig. 17. Cell edge throughput for increasing users.

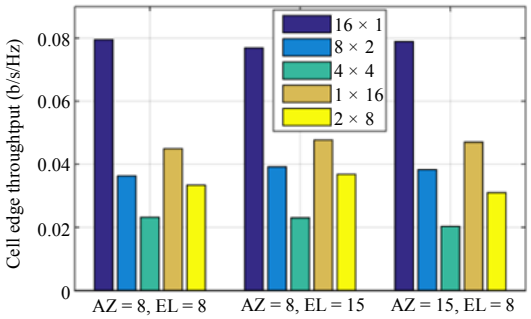

Fig. 18. Cell edge throughput for different angular spread scenarios.

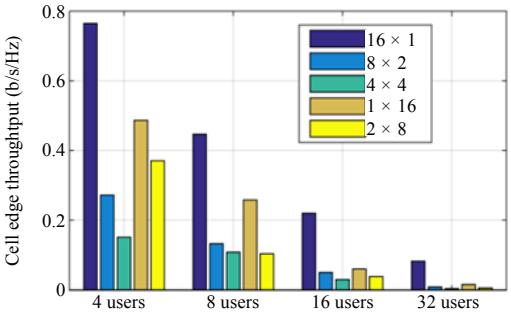

Fig. 19. Cell edge throughput for increasing users.

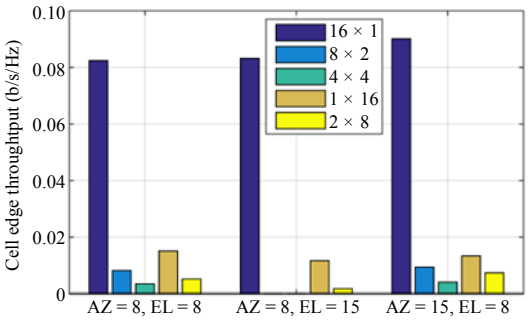

Fig. 20. Cell edge throughput for different angular spread scenarios.

(eAoDs below the reference boresight direction) showed better performance compared to that for a 90° angular spread.

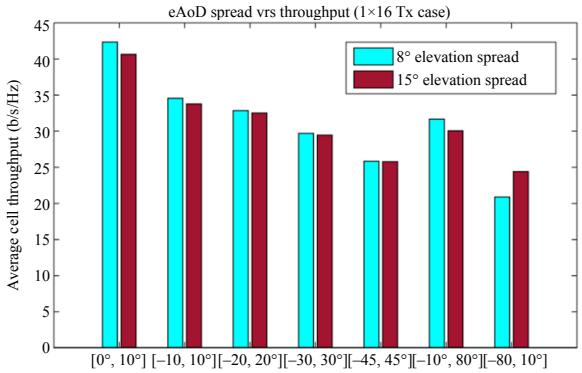

Fig. 21. Throughput for varying elevation spreads.

Table 3. Summary of results.

Channel	Performance trend (cell throughput)	Best antenna configuration for cell edge
No elevation restriction (reference model)	4 × 4 > 8 × 2 > 2 × 8 > 16 × 1 > 1 × 16	1 × 16 for high elevation spread 16 × 1 for low elevation spread
Urban model with eAoD restriction	1 × 16 > 2 × 8 > 4 × 4 > 8 × 2 > 16 × 1	16 × 1 for all angular spread scenarios
Suburban model	4 × 4 > 8 × 2 > 2 × 8 > 16 × 1 > 1 × 16	16 × 1 for all angular spread scenarios
Urban model with high LOS	1 × 16 > 2 × 8 > 4 × 4 > 8 × 2 > 16 × 1	16 × 1 for all angular spread scenarios

V. Conclusion

We implemented an eAoD range restriction technique to simulate the over-rooftop propagation that occurs in actual urban channels. The main results are summarized in Table 3. Typically, a wider angular spread leads to a lower correlation and high interference, resulting in low signal received power and thus reduced throughput. However, the vertical configuration with angular restriction was shown in this paper as being possibly more attractive than the horizontal configurations for most environment scenarios because it provides better performance in terms of user throughput. Knowledge of these conditions can help in selecting various antenna parameters and configurations that exploit the wireless channel in order to provide optimal performance.

References

[1] L. Vuokko et al., "Results from 5.3 GHz MIMO Measurement Campaign," COST 273 TD (04) 193, Duisburg, Germany, 2004.

[2] A. Kammoun et al., "Preliminary Results on 3D Channel Modeling: From Theory to Standardization," *IEEE J. Sel. Areas Commun.*, vol. 32, no. 6, June 2014, pp. 1219–1229.

[3] T. Taga, "Analysis for Mean Effective Gain of Mobile Antennas in Land Mobile Radio Environments," *IEEE Trans. Veh. Technol*., vol. 39, no. 2, May 1990, pp. 117–131.

[4] M. Shafi et al., "The Impact of Elevation Angle on MIMO Capacity," *IEEE Int. Conf. Commun.*, Istanbul, Turkey, June 11–15, 2006, pp. 4155–4160.

[5] Wireless World Initiative New Radio, "WINNER+ Final Channel Models," 2010.

[6] A. Abubakari, S. Raymond, and H. Jo, "Full Dimension MIMO Antenna Configuration for Optimal Performance," *Int. Conf. Inform. Commun. Technol. Convergence*, Jeju, Rep. of Korea, Oct. 28–30, 2015, pp. 1025–1030.

[7] 3GPP TR 25.996 V12.0.0, *Universal Mobile Telecommunications System (UMTS); Spatial Channel Model for Multiple Input Multiple Output (MIMO) Simulations*, ETSI, Sophia Antipolis Cedex, France, Sept. 2014.

[8] F. Pei, J. Zhang, and C. Pan, "Elevation Angle Characteristics of Urban Wireless Propagation Environment at 3.5 GHz," *IEEE Veh. Technol. Conf. (VTC Fall)*, Las Vegas, NV, USA, Sept. 2–5, 2013, pp. 1–5.

[9] Q. Luo et al., "3D MIMO Channel Model Based on Field Measurement Campaign for UMa Scenario," *IEEE Wireless Commun. Netw. Conf.*, Istanbul, Turkey, Apr. 6–9, 2014, pp. 171–176.

[10] C. Pan and J. Zhang, "Experimental Investigation of Elevation Angles and Impacts on Channel Capacity in Urban Microcell," *Int. Conf. Comput. Netw. Commun.*, Anaheim, CA, USA, Feb. 16–19, 2015, pp. 11–15.

[11] T. Kang and H. Kim, "Optimal Beam Subset and User Selection for Orthogonal Random Beamforming," *IEEE Commun. Lett.*, vol. 12, no. 9, Sept. 2008, pp. 636–638.

[12] P.A. Dighe, R.K. Mallik, and S.S. Jamuar, "Analysis of Transmit-Receive Diversity in Rayleigh Fading," *IEEE Trans. Commun*., vol. 51, no. 4, Apr. 2003, pp. 694–703.

[13] Y. Li et al., "An Enhanced Beamforming Algorithm for Three Dimensional MIMO in LTE-Advanced Networks," *Int. Conf. Wireless Commun. Signal Process.*, Hangzhou, China, Oct. 24–26, 2013, pp. 24–26.

[14] 3GPP doc. R1-071511, *Results on Zero-Forcing MU-MIMO*, Freescale Semiconductor Inc., 2007.

[15] D.J. Love and R.W. Heath, "Equal Gain Transmission in Multiple-input Multiple-output Wireless Systems," *IEEE Trans. Commun.*, vol. 51, no. 7, July 2003, pp. 1102–1110.

[16] B. Clerckx, G. Kim, and S. Kim, "Correlated Fading in Broadcast MIMO Channels: Curse or Blessing?" *IEEE Global Telecommun. Conf.*, New Orleans, LA, USA, Nov. 30–Dec. 4, 2008, pp. 1–5.

[17] D. Ying et al., "Kronecker Product Correlation Model and Limited Feedback Codebook Design in a 3D Channel Model," *IEEE Int. Conf. Commun.*, Sydney, Australia, June 10–14, 2014, pp. 5865–5870.

[18] Y. Xie et al., "A Limited Feedback Scheme for 3D Multiuser MIMO Based on Kronecker Product Codebook," *IEEE Annu. Int. Symp. Personal Indoor Mobile Radio Commun.*, London, UK, Sept. 8–11, 2013, pp. 1130–1135.

[19] J. Zhu et al., "Investigation on Precoding Techniques in E-UTRA and Proposed Adaptive Precoding Scheme for MIMO Systems," *Asia-Pacific Conf. Commun.*, Tokyo, Japan, Oct. 14–16, 2008, pp. 1–5.

[20] ITU-R M.2135-1, *Guidelines for Evaluation of Radio Interface Technologies for IMT-Advanced*, ITU, Geneva, Switzerland, Dec. 2009.

[21] WINNER II Channel Models, Deliverable D1.1.2 V1.2, IST-4-027756 WINNER II Deliverable, Feb. 2008.

[22] WINNER+ Final Channel Models, Deliverable D5.3 V1.0, June 2010.

[23] K.I. Pedersen, P.E. Mogensen, and B.H. Fleury, "A Stochastic Model of the Temporal and Azimuthal Dispersion Seen at the Base Station in Outdoor Propagation Environments," *IEEE Trans. Veh. Technol.*, vol. 49, no. 2, Mar. 2000, pp. 437–447.

[24] L.J. Greenstein et al., "A New Path-Gain/Delay-Spread Propagation Model for Digital Cellular Channels," *IEEE Trans. Veh. Technol.*, vol. 46, no. 2, May 1997, pp. 477–485.

[25] C. Cheon, G. Liang, and H.L. Bertoni, "Simulating Radio Channel Statistics for Different Building Environments," *IEEE J. Sel. Areas Commun.*, vol. 19, no. 11, Nov. 2001, pp. 2191–2200.

[26] A. Algans, K.I. Pedersen, and P.E. Mogensen, "Experimental Analysis of the Joint Statistical Properties of Azimuth Spread, Delay Spread, and Shadow Fading," *IEEE J. Sel. Areas Commun.*, vol. 20, no. 3, Apr. 2002, pp. 523–531.

[27] N.C. Beaulieu, A.A. Abu-Dayya, and P.J. McLane, "Estimating the Distribution of a Sum of Independent Lognormal Random Variables," *IEEE Trans. Commun.*, vol. 43, no. 12, Dec. 1995, pp. 2869–2873.

[28] Y. Nam et al., "Full-Dimension MIMO (FD-MIMO) for Next Generation Cellular Technology," *IEEE Commun. Mag*., vol. 51, no. 6, June 2013, pp. 172–179.

Alidu Abubakari received his BS degree in telecommunication engineering from the Kwame Nkrumah University of Science and Technology, Kumasi, Ghana, in 2013, and his MS degree in electronic engineering from Hanbat National University, Daejeon, Rep. of Korea, in 2016, where he is pursuing a PhD degree in electronic engineering. He is currently a researcher in substation automation and smart grid communication at Korea Electric Power Company, Daejeon, Rep. of Korea. His research interests include distributed massive MIMO networks (3D spatial channel modeling, beamforming, and SDMA), cloud radio access networks, small cells, smart grids, and heterogeneous networks.

Sabogu-Sumah Raymond was born in Ghana. He received his BS degree in telecommunications engineering (First Class Hons) from the Kwame Nkrumah University of Science and Technology, Kumasi, Ghana, in 2013. He is currently pursuing his MS degree at Hanbat National University, Daejeon, Rep. of Korea. He was with Huawei Technologies and National Communications Authority, both in Ghana, as a network optimization and telecommunications engineer, respectively. His research interests include spectrum sharing, coexistence between wireless services, millimeter wave communications, and cognitive radio networks.

Han-Shin Jo received his BS, MS, and PhD degrees in electrical and electronics engineering from Yonsei University, Seoul, Rep. of Korea, in 2001, 2004, and 2009, respectively. He is currently an associate professor with the Department of Electronics and Control Engineering, Hanbat National University, Daejeon, Rep. of Korea. He was a postdoctoral research fellow with the Wireless Network and Communications Group, Department of Electrical and Computer Engineering, University of Texas at Austin, USA from 2009 to 2011. He developed a long-term evolution base station in Samsung Electronics, Suwon, Rep. of Korea from 2011 to 2012. His current research interests are all aspects of MIMO (channel modeling, precoding and scheduling with limited feedback, beamforming, SDMA, and massive MIMO) and applications of stochastic geometry and optimization theory to wireless cellular and ad hoc networks. He received the Samsung Electronics Graduate Fellowship from 2006 to 2008, the Korea Research Foundation BrainKorea21 Graduate Fellowship from 2006 to 2007, the Korea Research Foundation Post-Doctoral Fellowship in 2009, and the 2011 ETRI Journal Best Paper Award.